*Materials Transactions*, Vol. 46, No. 5 (2005) pp. 1070 to 1078

**EXPRESS REGULAR ARTICLE**

# Beta TiNbSn Alloys with Low Young's Modulus and High Strength

Hiroaki Matsumoto, Sadao Watanabe and Shuji Hanada

*Institute for Materials Research, Tohoku University, Sendai 980-8577, Japan*

Young's modulus and tensile strength were investigated in relation to phase transformation and microstructural changes occurring during cold rolling and subsequent heat treatment using $\beta$ (Ti–35 mass%Nb)–4 mass%Sn and (Ti–35 mass%Nb)–7.9 mass%Sn alloys. Stress-induced $\alpha''$ martensite is generated on cold rolling of (Ti–35Nb)–4Sn whose martensitic transformation start temperature is around room temperature. Young's modulus in the rolling direction is lowered by the generation of stress induced $\alpha''$ phase with preferred texture, while it is recovered by the reverse martensitic transformation to $\beta$ at 523 K. The reverse transformation yields fine $\beta$ grains which are elongated approximately along the rolling direction and have an average grain size in width of less than 1 μm. This fine microstructure leads to high strength over 800 MPa with keeping low static Young's modulus of 43 GPa. In contrast, mechanical properties of (Ti–35Nb)–7.9Sn in which matensite is not stress-induced are not so significantly improved by cold rolling and heat treatment.

(Received December 28, 2004; Accepted April 11, 2005; Published May 15, 2005)

***Keywords:*** *Young's modulus, strength, titanium–niobium–tin alloy, stress induced $\alpha''$ martensite, texture, thermo-mechanical processing, fine grained microstructure*

## 1. Introduction

In metastable $\beta$ Ti alloys, their Ms temperature is below room temperature and high temperature $\beta$ phase can be retained at room temperature by quenching. The deformation of this $\beta$ phase involves slip, $\{332\}\langle 113\rangle$ twinning and stress-induced martensitic transformation, depending on the stability of $\beta$ phase.[1–4] Crystallographic slip occurs in alloys with high stability of $\beta$ phase, while stress-induced martensitic transformation and $\{332\}\langle 113\rangle$ twinning are formed in unstable $\beta$ phase alloys. Especially, the twinning is known to form in unstable $\beta$ phase containing finely distributed athermal $\omega$ phase particls.[1,2] These different deformation modes were found to strongly affect their mechanical properties like strength and ductility. Recently, Ozaki *et al.* have demonstrated that Young's modulus of $\beta$ TiNbSn alloys consisting of non-cytotoxic elements is closely associated with the stability of $\beta$ phase in relation to $\omega$ transformation and $\alpha''$ martensitic transformation, and low Young's modulus of about 39 GPa close to that of human bone (10–30 GPa) is obtained at room temperature by optimizing the alloy composition.[5] This low value of Young's modulus indicates that the $\beta$ TiNbSn alloy is promising as biomedical implants such as stems for artificial hip joints and orthopedic bone plates. However, high strength as well as low Young's modulus is required for the implants subjected to cyclic loading under complicated stress conditions.[6,7] It is widely recognized that low Young's modulus originating from low bonding strength between atoms in an alloy leads to low mechanical strength of the alloy. Therefore, a method should be developed to strengthen $\beta$ Ti alloys without sacrificing low Young's modulus. Precipitation hardening, which is one of typical strengthening mechanisms in alloys, may be ruled out to achieve simultaneously both low Young's modulus and high strength, because it generally results in an increase in Young's modulus in many alloys.

This work aims at investigating whether the strength of low Young's modulus TiNbSn alloy can be increased by microstructure control without increasing Young's modulus.

## 2. Experimental Procedure

Ti–Nb–Sn alloys with compositions of (Ti–35 mass%Nb)–4 mass%Sn and (Ti–35 mass%Nb)–7.9 mass%Sn were prepared by arc melting in an argon atmosphere using high purity Ti, Nb and Sn. The composition ratio of Ti and Nb was fixed by 65 mass% and 35 mass%, respectively, and then Sn was added. Since weight changes before and after the arc-melting were negligible, the alloy compositions will be denoted hereafter by nominal compositions abbreviated as (Ti–35Nb)–4Sn and (Ti–35Nb)–7.9Sn. The arc-melted buttons were homogenized at 1423 K for 86.4 ks, solution treated at 1223 K for 7.2 ks in an evacuated quartz tube, and then quenched into ice water. The solution treated buttons were cold rolled at reductions of 66 and 89% so as to have the final thickness of 1.0 mm. The cold rolled specimens will be called 66 and 89% CR hereafter, respectively. The 89% CR specimens were heat-treated at temperatures from 423 to 573 K for 7.2 ks. The specimens heat-treated at 423, 473, 523 and 573 K will be called 423, 473, 523 and 573 K HT, respectively. The cold rolled specimens at the reduction of 89% were solution treated at 1223 K for 1.8 ks and quenched into ice water. Finally solution treated specimens will be called ST. Samples for the measurement of anisotropy of Young's modulus were prepared by 89% cold rolling after furnace cooling of arc-melted buttons homogenized at 1423 K for 86.4 ks (89% CRY) and solution treatment at 1223 K for 7.2 ks followed by quenching into ice water (STY). These thermo-mechanical processing schedules are as shown in Table 1. Martensitic transformation temperature was measured by differential scanning calorimetry (DSC). Microstructures were identified by X-ray diffraction (XRD), optical microscopy (OM) and Orientation Imaging Microscopy (OIM). Grain orientations were measured at a step size of 0.25 μm using Philips XL 30 FEG SEM equipped with OIM of TexSEM Laboratories. Textures were examined using an X-ray texture goniometer by Cu K$\alpha$ radiation. The pole figures were measured within the range of the distance angle 0–70° in the back reflection method. Dynamic Young's modulus was measured at room temperature (298 K) mainly by the free resonance vibration

Table 1 Classification of thermo-mechanical processing in this work.

| | | | | | |
|---|---|---|---|---|---|
| Arc melted ingot (t=8.9mm) | Homogenized treatment (1423K–86.4ks) | Solution treatment (1223K–7.2ks) | Cold rolling (t=1.0mm) 89% CR | Heat treatment (423~573K–7.2ks) HT | |
| | | | | Solution treatment (1223K–1.8ks) ST | |
| | | Cold rolling (t=3.0mm) | Solution treatment (1223K–7.2ks) | Cold rolling (t=1.0mm) 66% CR | |
| | | | Cold rolling (t=1.0mm) 89% CRY | Heat treatment (423~573K–7.2ks) HTY | |
| | | | | Solution treatment (1223K–1.8ks) STY | |

* t: thickness of specimen

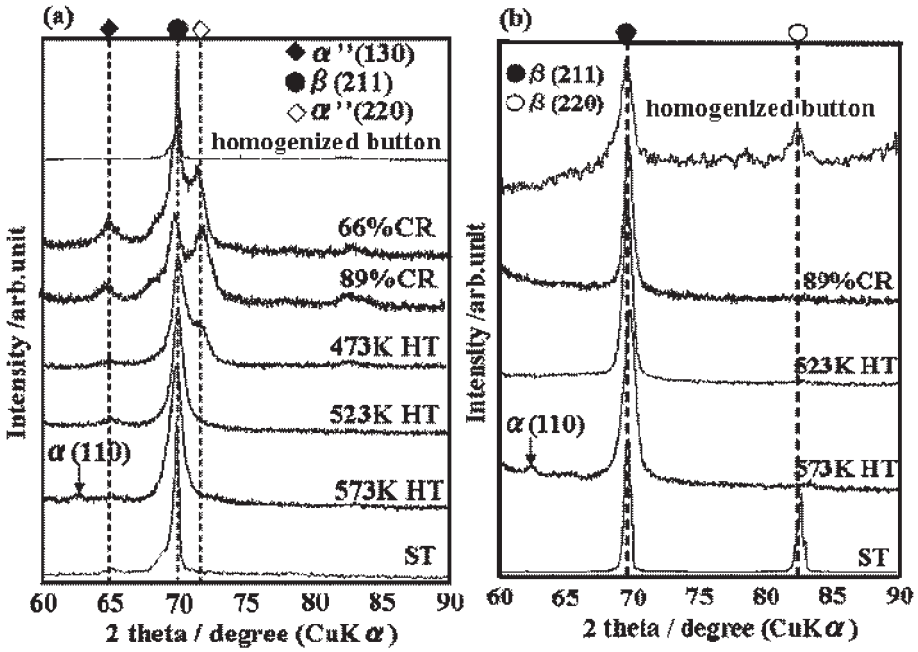


Fig. 1 Phase evolution by cold rolling and heat treatment obtained from XRD analysis. (a) (Ti–35 mass%Nb)–4 mass%Sn and (b) (Ti–35 mass%Nb)–7.9 mass%Sn.

method using a sample with dimensions 10 mm × 50 mm × 1 mm. Static Young's modulus was also measured at various temperatures from 233 to 423 K by tensile test at a strain rate of $6.7 \times 10^{-5}\,s^{-1}$, where tensile strain was directly measured by a CCD camera. Tensile strength was also examined by tensile test at an initial strain rate of $1.5 \times 10^{-4}\,s^{-1}$.

## 3. Results and Discussion

### 3.1 Phase evolution under cold rolling

Figure 1 shows the XRD profiles of homogenized, cold rolled, heat treated and solution treated (Ti–35Nb)–4Sn (a) and Ti–35Nb–7.9Sn (b). As shown in Fig. 1(a), homogenized (Ti–35Nb)–4Sn is composed of a $\beta$ (bcc) single phase, while two phases of $\beta$ and $\alpha''$ (orthorhombic) martensite are clearly seen after cold rolling (66 and 89% CR). The peak intensity ratio of $(220)_{\alpha''}$ to $(211)_{\beta}$ is seen to increase with increasing cold rolling reduction. This observation indicates that stress-induced martensitic transformation occurs by cold rolling and is enhanced on further cold rolling. On the other hand, a single $\beta$ phase is identified in homogenized and cold rolled (89% CR) (Ti–35Nb)–7.9Sn, as shown in Fig. 1(b). A very weak $\alpha''$ peak is observed in ST (Ti–35Nb)–4Sn, while not in ST (Ti–35Nb)–7.9Sn. DSC analysis revealed that Sn addition to Ti–Nb alloys decreases martensitic transformation start temperature (Ms) in good agreement with a previous paper.[8] That is, Ms is about 308 K for ST (Ti–35Nb)–4Sn, whereas it is lower than 223 K for ST (Ti–35Nb)–7.9Sn. Figure 2 shows

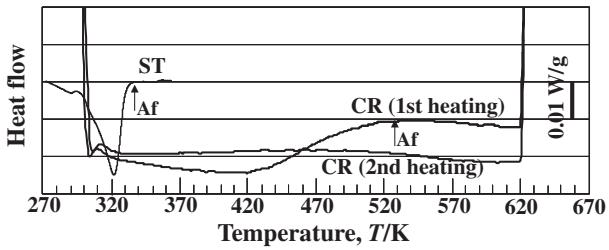


Fig. 2 DSC heating curves of (Ti–35 mass%Nb)–4.0 mass%Sn cold rolled and solution treated.

the DSC heating curves of ST (Ti–35Nb)–4Sn and CR (Ti–35Nb)–4Sn. The DSC curve for ST was measured in heating after cooling to 173 K at which martensitic transformation was completed. One can see clearly the reverse martensitic transformation corresponding to an endothermic peak and Af of ST can be unambiguously determined to be 335 K. On the other hand, the DSC curves for CR were measured in heating after cold rolling at from room temperature to 623 K for two cycles. No sharp endothermic peak can be detected for CR, but weak endothermic behavior appears only for the first heating. Taking the result of XRD (Fig. 1) into consideration, the endothermic behavior for the first heating will correspond to the reverse martensitic transformation of stress induced martensite generated by cold rolling, and Af can be estimated to be at around 530 K. The cause of the broad endothermic peak in the DSC curve is not well understood at present, but one possible explanation is that various martensite variants produced by solution treatment and rolling are further deformed by the subsequent rolling and consequently individual variants have different substructures. This explanation is based on the observation that the broadening was enhanced with increasing cold rolling reduction. It is interesting to note in Figs. 1(a) and 2 that the stress-induced $\alpha''$ martensite is still observed in 473 K HT (Ti–35Nb)–4Sn, although Af was 335 K for ST (Ti–35Nb)–4Sn, and almost completely disappears after heat treatment at 523 K. These results display that the reverse martensitic transformation is retarded by cold rolling, suggesting that martensite formed by cold rolling is stabilized.

### 3.2 Young's modulus

Figure 3 shows the dynamic Young's modulus in the rolling direction of ST, 89%CR, 523 and 573 K HT for (Ti–35Nb)–4Sn and (Ti–35Nb)–7.9Sn. Young's modulus in (Ti–35Nb)–4Sn decreases from 55 GPa of ST (main phase: $\beta$ phase) to 42 GPa of 89% CR (main phases: $\beta + \alpha''$), implying that Young's modulus of $\alpha''$ martensite is lower than that of $\beta$ phase. Although several authors discussed the values of Young's moduli for single phase $\alpha''$, $\beta$ and $\omega$, they have drawn contradictory conclusions except for the highest value of $\omega$ phase.[5,7,9,10] Young's modulus of $\alpha''$ martensite will be discussed later. As seen in Fig. 3, the decreased Young's modulus by cold rolling in (Ti–35Nb)–4Sn is recovered close to the initial value of 53 GPa by heat treatment at 523 K, where the reverse martensitic transformation is almost completed from XRD and DSC analysis. These results suggest that the recovery of Young's modulus to the value of

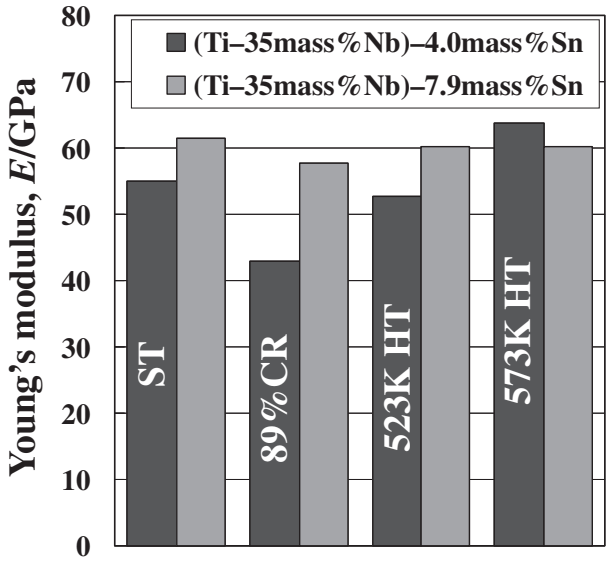


Fig. 3 Dynamic Young's modulus of (Ti–35 mass%Nb)–4 mass%Sn and (Ti–35 mass%Nb)–7.9 mass%Sn at various conditions.

ST under heat treatment after cold rolling is strongly related to the reversion of stress induced martensite. On the other hand, Young's modulus increases to a higher value of 64 GPa by heat treatment at 573 K, where $\alpha$ precipitation occurs as shown in Fig. 1(a). In contrast, no significant change in Young's modulus can be seen in cold rolled and heat treated (Ti–35Nb)–7.9Sn. Quite recently, Ozaki *et al.* have shown that precipitation of athermal or isothermal $\omega$ phase in $\beta$ Ti alloys increases Young's modulus, and low Young's modulus of $\beta$ TiNb alloys can be achieved by Sn addition which retards or suppresses $\omega$ precipitation in unstable $\beta$ phase.[5] It is obvious, therefore, that no significant $\omega$ transformation is caused during cold rolling and heat treatment at 523 K for 7.2 ks.

Figure 4 shows dynamic Young's modulus at room temperature in the rolling direction and Ms temperature for (a) solution treated Ti–Nb binary alloys as a function of Nb content and (b) solution treated (Ti–35 mass%Nb)–$x$ mass%Sn alloys as a function of Sn content. Young's modulus exhibits a minimum at Nb content of 42 mass%Nb for the binary alloys and around Sn content of 4 mass%Sn for the ternary alloys. It should be noted that Ms temperature at the composition corresponding to the minimum is close to room temperature, as shown in Figs. 4(a) and (b). Young's modulus below the minimum compositions increases with decreasing Nb or Sn content, or with increasing volume fraction of $\alpha''$ martensite. This tendency seems to be inconsistent with the result in Fig. 3, where Young's modulus decreases with increasing volume fraction of $\alpha''$. According to TEM observation, however, the intensity of athermal $\omega$ reflections in retained $\beta$ phase increases with decreasing Nb or Sn content, thereby leading to an increase of Young's modulus in fine $\omega$ particle-containing $\beta$ phase. Therefore, the present result suggests that Young's modulus of $\beta$ Ti alloys should be discussed by considering not only volume fractions of $\beta$ and $\alpha''$ phases but also $\omega$ transformation in retained $\beta$ phase.

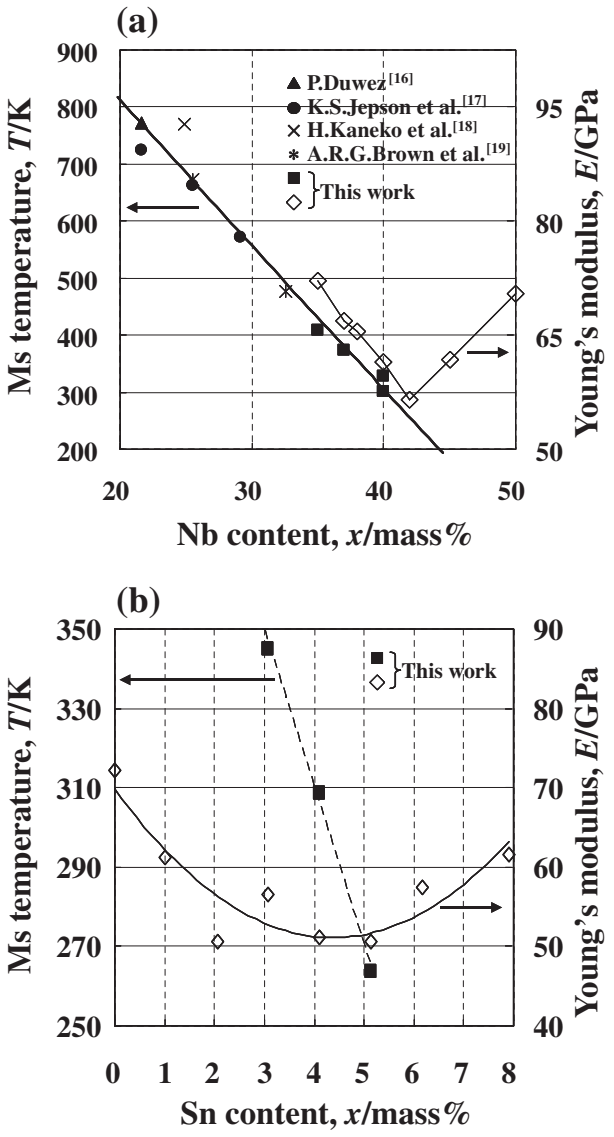


Fig. 4 Composition dependence of Ms temperature and dynamic Young's modulus as a function of (a) Nb content in Ti–Nb binary alloys and (b) Sn content in (Ti–35 mass%Nb)–$x$ mass%Sn alloys.

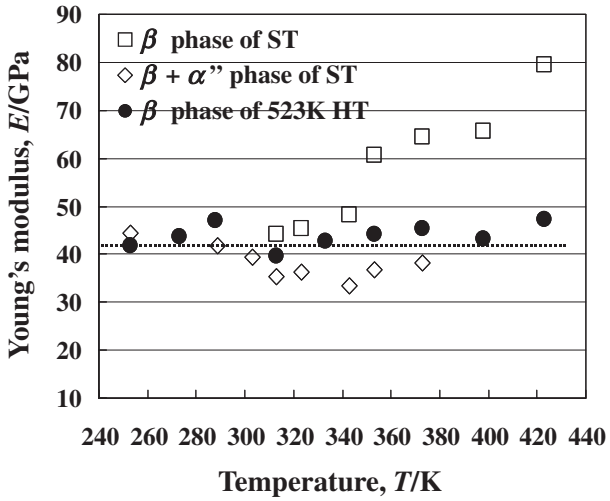


Fig. 5 Temperature dependence of static Young's modulus obtained by tensile test of (Ti–35 mass%Nb)–4 mass%Sn solution treated and heat treated at 523 K.

Figure 5 shows the temperature dependence of static Young's modulus in the rolling direction of ST and 523 K HT (Ti–35Nb)–4Sn alloy, which is obtained from true stress–true strain curves in tensile test. Young's modulus of ST (open square symbols) decreases with decreasing temperature toward Ms of 308 K determined by DSC and becomes temperature-independent below Ms, as indicated by open diamond symbols. The open diamond symbols above Ms denote apparent Young's modulus obtained from linear work hardening region after initiation of stress-induced martensitic transformation. On the contrary, Young's modulus of 523 K HT (solid circles) is almost constant in the temperature range investigated. It is generally known that Young's modulus of metals and alloys increases with decreasing temperature, but this tendency is reversed when the parent phase is approaching Ms. Therefore, the temperature dependence of static Young's modulus for ST in Fig. 5 is attributable to the reduced stability of $\beta$ phase for $\alpha''$ martensitic transformation. Very interestingly, static Young's modulus of 523 K HT is independent of temperature. In addition, no stress-induced $\alpha''$ martensite was detected after deformation below room temperature. Also, no DSC peak was seen in cooling below room temperature. These results strongly suggest that $\beta$ phase generated by reverse martensitic transformation is stabilized, and consequently low Young's modulus can be attained in a wide temperature range above and below room temperature. Here, it is noted that the static Young's modulus values of 523 K HT in Fig. 5 are lower (43 GPa on an average) than the dynamic value (53 GPa) in Fig. 3. Such a difference between static and dynamic Young's modulus values has been found in many alloys, but details are unknown at present.

Figure 6 shows $\{110\}_\beta$ and $\{211\}_\beta$ pole figures in the rolling plane of $\beta$ phase in (a) ST (Ti–35Nb)–4Sn and (b) ST (Ti–35Nb)–7.9Sn. The preferred texture is $\{211\}_\beta\langle 110\rangle_\beta$ for both the alloys and a weak texture of $\{110\}_\beta\langle 112\rangle_\beta$ is seen only in ST (Ti–35Nb)–7.9Sn. Figure 7 shows $\{110\}_\beta$ and $\{100\}_\beta$ pole figures in the rolling plane for $\beta$ phase of (a) 89% CR (Ti–35Nb)–4Sn and (b) 89% CR (Ti–35Nb)–7.9Sn. Preferred $\{211\}_\beta\langle 110\rangle_\beta$ and $\{100\}_\beta\langle 110\rangle_\beta$ textures can be seen in the $\beta$ phase of both the alloys. The former texture is much stronger than the latter one in (Ti–35Nb)–4Sn, whereas the texture preference in (Ti–35Nb)–7.9Sn is reversed between the two textures. Figure 8 shows (a) $(200)_{\alpha''}$ pole figure in the rolling plane and (b) $(020)_{\alpha''}$ pole figure in the cross section perpendicular to the rolling direction for $\alpha''$ martensite in 89% CR (Ti–35Nb)–4Sn. Obviously, strong $(200)_{\alpha''}$ texture is observed in the rolling plane, and strong $(020)_{\alpha''}$ texture is seen in the cross section. Although an extremely weak $(110)_{\alpha''}$ texture is observed in the rolling plane, it will be disregarded in the following discussion. From these results in Figs. 7 and 8, $\alpha''$ martensite of 89% CR (Ti–35Nb)–4Sn is found to have strong $(200)_{\alpha''}[010]_{\alpha''}$ texture. This texture is in good agreement with the result by Baker.[11] As described above, since the $\beta$ phase of 89% CR (Ti–35Nb)–4Sn has preferred $\{100\}_\beta\langle 110\rangle_\beta$, it is most likely that the well-known lattice correspondence of $[100]_{\alpha''} \parallel \langle 100\rangle_\beta$, $[010]_{\alpha''} \parallel \langle 101\rangle_\beta$ and $[001]_{\alpha''} \parallel \langle 110\rangle_\beta$[12,13] holds between $\{100\}_\beta\langle 110\rangle_\beta$ and $(200)_{\alpha''}[010]_{\alpha''}$. Considering

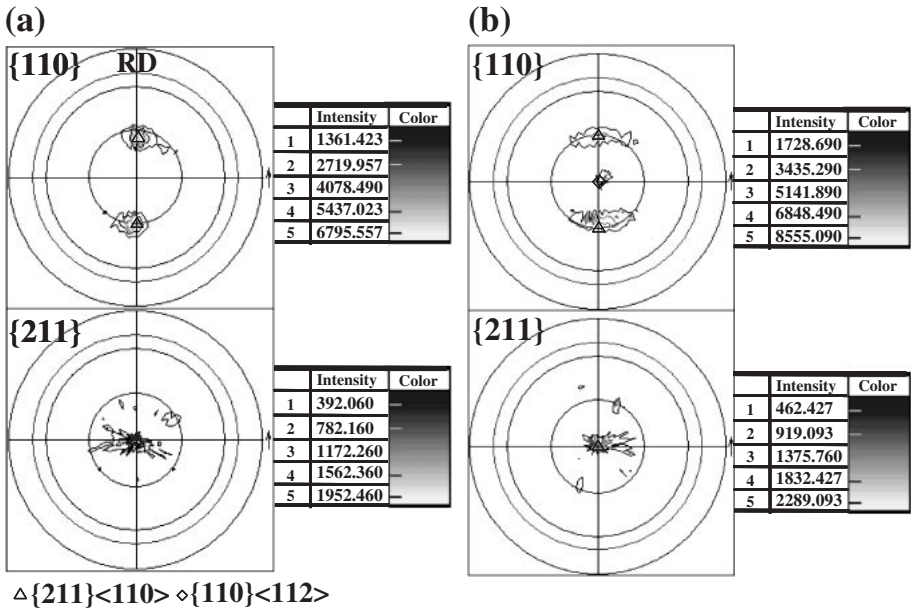


Fig. 6 Pole figures in the rolling plane for $\beta$ of solution treated (a) (Ti–35 mass%Nb)–4 mass%Sn and (b) (Ti–35 mass%Nb)–7.9 mass%Sn.

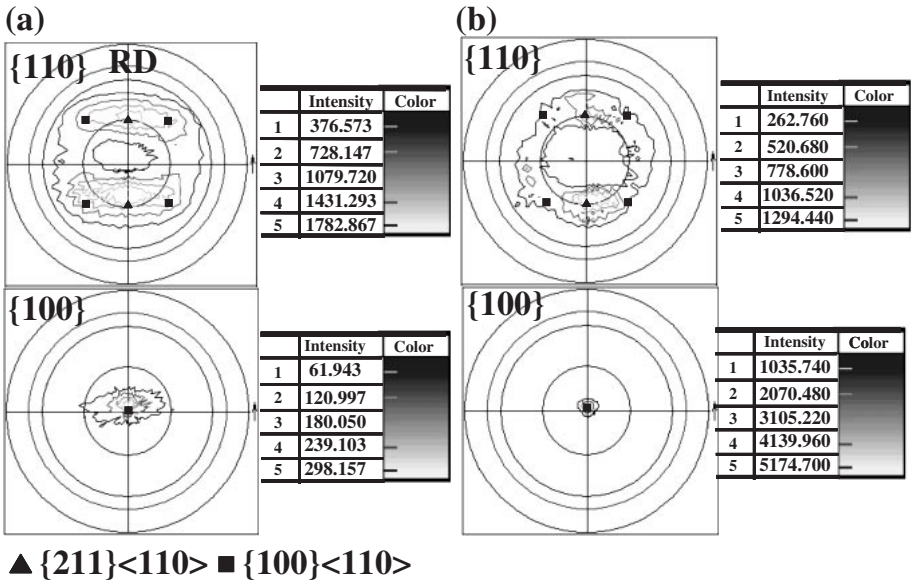


Fig. 7 Pole figures in the rolling plane for $\beta$ of 89% cold rolled (a) (Ti–35 mass%Nb)–4 mass%Sn and (b) (Ti–35 mass%Nb)–7.9 mass%Sn.

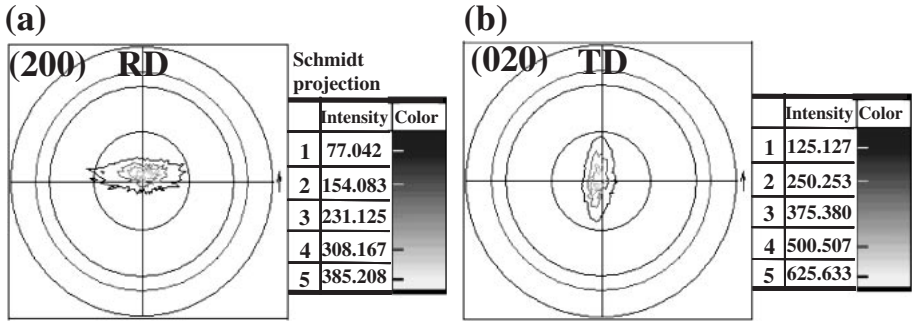


Fig. 8 Pole figures for $\alpha''$ of 89% cold rolled (Ti–35 mass%Nb)–4 mass%Sn (a) in the rolling plane and (b) in the cross section perpendicular to the rolling direction.

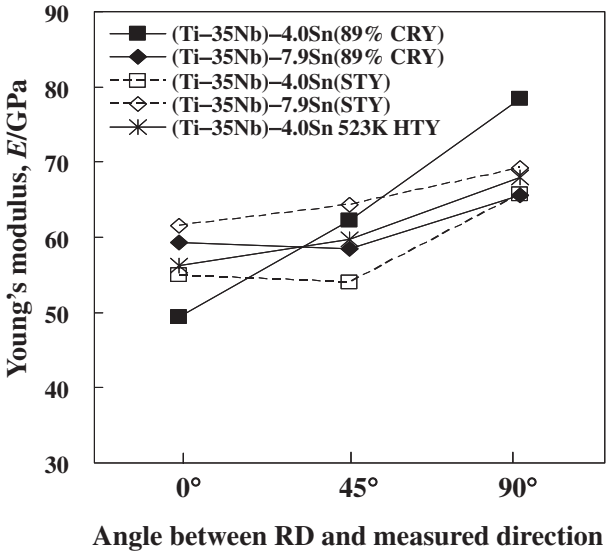


Fig. 9 Dynamic Young's modulus in 89% cold rolled, solution treated and 523 K HT (Ti–35 mass%Nb)–4 mass%Sn and (Ti–35 mass%Nb)–7.9 mass%Sn.

this lattice correspondence, the strong $(200)_{\alpha''}[010]_{\alpha''}$ martensite variant would be generated with close relation to $\{100\}_\beta\langle 110\rangle_\beta$, although $\{211\}_\beta\langle 110\rangle_\beta$ texture is also observed. This preferential formation of the stress induced martensite variant will be discussed later. It is noted that the spread of $[100]_{\alpha''}$ pole to the transverse direction (TD) in Fig. 8(a) is associated with the spread of $[100]_\beta$ pole to TD in Fig. 7(a). However, the spread of $[010]_{\alpha''}$ pole to TD in Fig. 8(b) cannot be caused by the spread of $[100]_\beta$ pole to TD which brings no dispersion of $[010]_{\alpha''}$ pole in Fig. 8(b). Instead, the spread of [110] pole to TD, which is associated with the spread of $\langle 211\rangle_\beta$ pole, is attributable to the spread of $[010]_{\alpha''}$ pole to TD in Fig. 8(b). Thus, it is strongly suggested that stress-induced martensite variants are deformed during cold rolling to generate texture by obeying the lattice correspondence between $\beta$ and $\alpha''$.

Figure 9 shows the dynamic Young's modulus as a function of angle from the rolling direction. Young's modulus of 89% CRY (Ti–35Nb)–4Sn exhibits remarkable anisotropy, as compared with STY (Ti–35Nb)–4Sn and STY (Ti–35Nb)–7.9Sn and 89% CRY (Ti–35Nb)–7.9Sn, and possesses the highest value at 90° direction. Slightly higher Young's modulus of 89% CRY (Ti–35Nb)–4Sn than that of 89%CR in Fig. 3 is due to the difference in heat treatment. Since encapsulation in a quartz tube for solution treatment was difficult for samples to measure Young's modulus in the transverse direction, homogenized samples were furnace cooled and then cold rolled. Hence decomposition of $\beta$ phase may occur slightly during furnace cooling. Considering the similar $\beta$ textures of 89% CRY (Ti–35Nb)–4Sn and (Ti–35Nb)–7.9Sn, the strong anisotropy of Young's modulus in the 89% CRY (Ti–35Nb)–4Sn would originate from the $\alpha''$ texture. It is well known that a few martensite variants can be preferentially formed on deformation, dependent on applied stress direction. Therefore, the observed anisotropy could be explained by assuming that $\alpha''$ has significant crystallographic anisotropy in Young's modulus and cold rolling generates preferential formation of $\alpha''$ variants in the rolling direction. As mentioned above, $\alpha''$ has the preferred orientation of $[010]_{\alpha''}$ in the rolling direction. Lattice parameters of $\alpha''$ for 89% CR (Ti–35Nb)–4Sn were determined by XRD as follows, although they could not be precisely determined because of peak broadening and cold rolling texture.

$$a_{\alpha''} = 0.325_9\,\text{nm}, \quad b_{\alpha''} = 0.485_9\,\text{nm}, \quad c_{\alpha''} = 0.465_2\,\text{nm}.$$

Clearly, $b_{\alpha''}$ is much larger than $c_{\alpha''}$. According to the lattice parameters of $\beta$ and $\alpha''$ measured precisely for solution treated $\beta$ Ti alloys, the lattice contracts in $[100]_{\alpha''}$ direction and expands in $[010]_{\alpha''}$ and $[001]_{\alpha''}$ directions with larger expansion in $[010]_{\alpha''}$ than in $[001]_{\alpha''}$ when the above-mentioned lattice correspondence is considered for $\beta$ to $\alpha''$ transformation. As described above, the strong preferential martensite texture of $(200)_{\alpha''}[010]_{\alpha''}$ is formed after 89% cold rolling. This is because the rolling direction coincides with the large expansion direction $[010]_{\alpha''}$ in the lattice correspondence of transformation. It is reasonable to assume, therefore, that Young's modulus is lower in the rolling direction with dominant texture $[010]_{\alpha''}$ than in the transverse direction with $[001]_{\alpha''}$ texture, since the distance between atoms is longer in $b_{\alpha''}$ in $[010]_{\alpha''}$ direction than in $c_{\alpha''}$ in $[001]_{\alpha''}$ direction. Furthermore, as shown in Fig. 9, the anisotropy of Young's modulus in cold rolled (Ti–35Nb)–4Sn is decreased by heat treatment for reverse martensitic transformation, implying that the formation of preferred martensitic variant causes the remarkable anisotropy.

Figure 10 shows the true stress–true strain curves of (Ti–35Nb)–4Sn for (a) 523 K HT tensile tested at 253, 288 and 373 K and (b) ST tensile tested at 373 K. When the stress–strain curves in Figs. 10(a) and (b) are compared at 373 K, a yielding point corresponding to the initiation of stress-induced martensitic transformation is observed in ST (Fig. 10(b)), but not in 523 K HT (Fig. 10(a)). Moreover, no yielding point is seen at much lower temperature, 288 and 253 K in 523 K HT. This result is well consistent with the decrease of Ms in agreement with the temperature independent Young's modulus in Fig. 5, suggesting that $\beta$ phase stabilization occurs in 523 K HT.

Figure 11 shows (a) the OM micrograph of ST and (b) the OIM image of 523 K HT for (Ti–35Nb)–4Sn. The ST micrograph in Fig. 11(a) consists of coarse, equiaxed grains containing a small amount of martensite plates around grain boundaries in agreement with XRD result in Fig. 1(a). Figure 11(b) shows the orientation distribution of $\beta$ grains in 523 K HT, which is drawn by color mapping with an orientation triangle inserted in Fig. 11. Near-{001} and -{211} grains can be well observed in the rolling plane in good agreement with the $\beta$ textures measured by XRD for 523 K HT. The average grain sizes of ST and 523 K HT determined by the intercept method at the transverse direction in Figs. 11(a) and (b) were 120 and 1.3 μm, respectively. Since small grains in black areas in Fig. 11(b) were not counted, actual grain size of elongated grains in width is estimated to be less than 1 μm. Thus, $\beta$ stabilization in 523 K HT will be caused by grain refinement. This type of stabilization has been reported in other alloys. Takai *et al.* have investigated the relationship between grain refinement

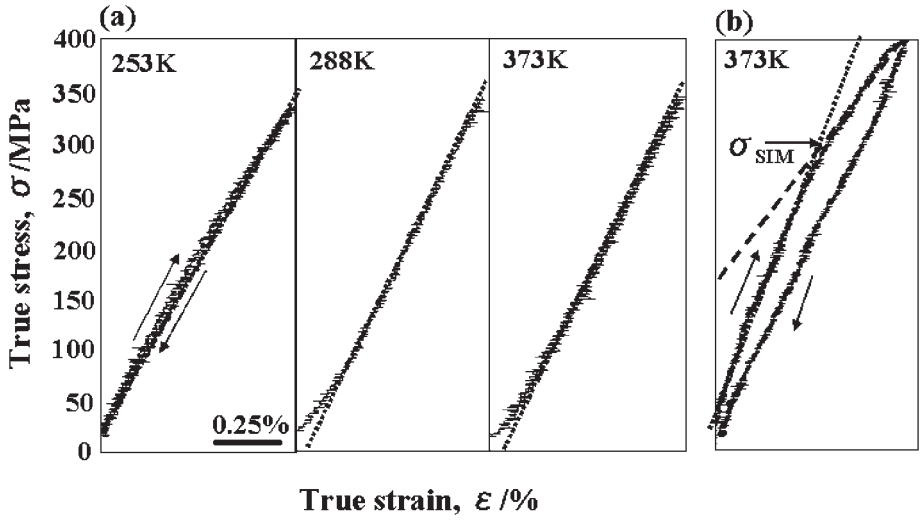


Fig. 10 True stress–true strain curves of (Ti–35 mass%Nb)–4 mass%Sn for (a) 523 K HT at 253, 288 and 373 K and (b) ST at 373 K.

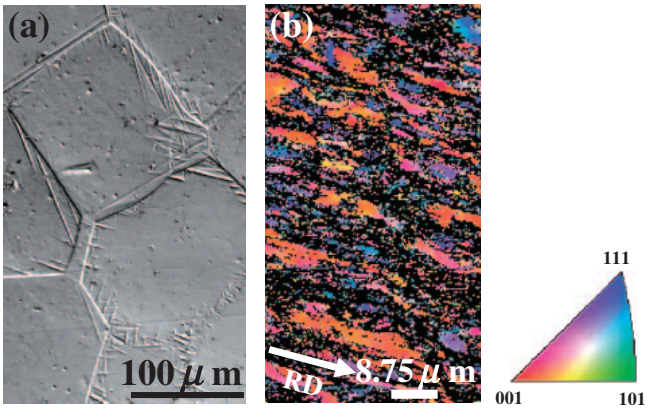


Fig. 11 Optical micrograph of ST (a) and OIM image of 523 K HT (Ti–35 mass%Nb)–4 mass%Sn which show the orientation distribution in (b).

by the reversion of deformation induced martensite and austenite stabilization by calculating physical energy required for martensitic transformation in Fe–16%Cr–10%Ni.[14] They pointed out that grain refinement of austenite to 1 μm or less is very effective to suppress martensitic transformation. Similar discussion has been reported by Hao *et al.* in metastable β Ti alloy.[7] Moreover, the compositional change accompanied by α precipitation under heat treatment should be also considered for the β stabilization in 523 K HT.

Considering the coarse grain sizes of 3 to 5 mm before cold rolling in the homogenized buttons in this study, further refinement of β grains formed by reverse martensitic transformation could be achieved by rolling at finer initial grains under higher cold rolling reductions.

### 3.3 Tensile properties

Figure 12 shows the nominal stress–nominal strain curves of CR, HT and ST for (a) (Ti–35Nb)–4Sn and (b) (Ti–35Nb)–7.9Sn. In (Ti–35Nb)–4Sn, double yielding followed by linear hardening and necking is observed in ST, while parabolic hardening followed by remarkable necking is seen in CR and HT. The first yielding in ST is attributable to stress-induced martensitic transformation and the second yielding will be associated with initiation of slip deformation in α″ martensite. The linear work hardening will result from fragmentation of β grains by dispersed martensite plates. The stress–strain curves of 89% CR and 423 K HT, which correspond to deformation of heavily strained β and α″ phases, are quite similar, implying that no significant microstructure change is

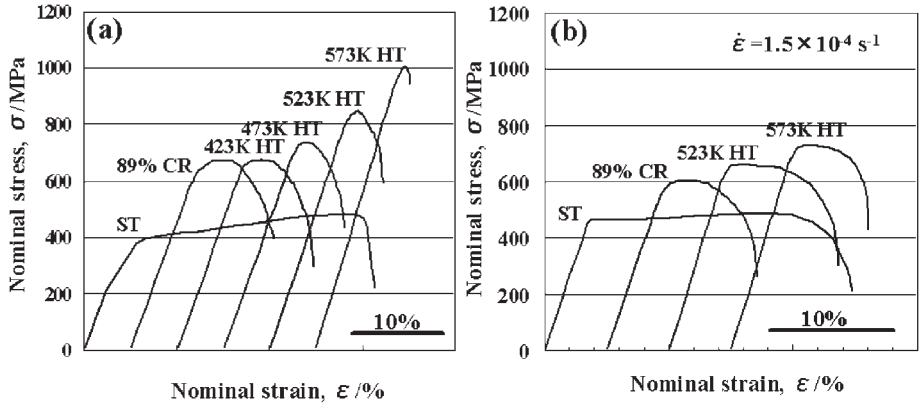


Fig. 12 Nominal stress–nominal strain curves of (a) (Ti–35 mass%Nb)–4.0 mass%Sn and (b) (Ti–35 mass%Nb)–7.9 mass%Sn at various conditions.

evolved in the heat treatment at 423 K after cold rolling. Tensile strength increases with further increasing heat treatment temperature. The highest tensile strength obtained in 573 K HT is due to the precipitation of $\alpha$ phase, as evidenced in Fig. 1(a) and also as suggested by the increase in Young's modulus in Fig. 3. In contrast, the increase in flow stress of 473 and 523 K HT is not clearly understood at present, because no new phase is detected from XRD in Fig. 1(a) and Young's modulus of 523 K HT is recovered almost completely as shown in Fig. 3. XRD result in Fig. 1(a) indicates that the reverse martensitic transformation occurs partially in 473 K HT and almost completely in 523 K HT. However, the increase in flow stress of 473 and 523 K HT cannot be related to the change in volume fractions of $\beta$ and $\alpha''$. This is because the yield stress of 89% CR (Ti–35Nb)–7.9Sn in which stress-induced martensitic transformation is not accompanied increases by heat treatment at 523 K as shown in Fig. 12(b). $\alpha$ precipitation was clearly observed in 573 K HT by XRD analysis as shown in Figs. 1(a) and (b). Hence, the increase in yield stress by heat treatment is attributable to $\alpha$ precipitation in (Ti–35Nb)–4Sn and (Ti–35Nb)–7.9Sn, even though $\alpha$ phase was not detected from XRD. Since $\beta$ phase cold rolled or formed by reverse martensitic transformation contains an extremely high density of dislocations, $\alpha$ phase will precipitate very finely on dislocations. These precipitates would increase tensile strength, but not significantly change Young's modulus. The recovery in Young's modulus of 523 K HT in Fig. 3 is considered to be due to disappearance of textured $\alpha''$ by the reverse martensitic transformation. Once $\alpha$ precipitation occurs, $\beta$ phase will be stabilized. This decomposition of $\beta$ phase is ascribed to $\beta$ stabilization in 523 K HT in addition to the grain refinement discussed above. Further studies are needed to clarify the correlation among Young's modulus, $\alpha$ precipitation and $\alpha''$ texture.

Elongation to fracture of (Ti–35Nb)–4Sn and (Ti–35Nb)–7.9Sn decreases by cold rolling and heat treatment. It should be noted that 523 K HT of (Ti–35Nb)–4Sn exhibits high strength over 800 MPa with an appreciable elongation to fracture of 6.5%. Figure 13 shows the tensile strength of ST, CR and HT for (Ti–35Nb)–4Sn and (Ti–35Nb)–7.9Sn. Tensile strengths of ST (Ti–35Nb)–4Sn and (Ti–35Nb)–7.9Sn exhibit almost the same value of about 500 MPa. Obviously, the increase in tensile strength by cold rolling and heat treatment is seen more prominently in (Ti–35Nb)–4Sn than in (Ti–35Nb)–7.9Sn. Work hardening by dislocation interaction, microstructure refinement by martensite formation and enhanced $\alpha$ precipitation arising from unstable $\beta$ phase are responsible for the strength increase in (Ti–35Nb)–4Sn.

It is generally accepted that grain growth in many $\beta$ Ti alloys is very fast above the $\beta$ transus temperature and hence the refinement of $\beta$ grains through thermo-mechanical processing is not so easy. However, the simple process presented in this work allows to provide fine $\beta$ grains resulting in high strength and is applicable to other $\beta$ Ti alloy systems. By optimizing alloy composition and thermo-mechanical processing conditions, mechanical properties such as Young's modulus and strength will be further improved. Such studies are underway.

The strength to modulus ratio is used as the barometer of material-performance for biomedical Ti alloy implants; the higher this ratio, the more desirable the materials for such applications.[15] Figure 14 shows the strength to modulus ratio of ST, CR and HT for (Ti–35Nb)–4Sn in comparison with several commercial implant materials. The highest strength to modulus ratio of about 16 is obtained for 523 K HT in this work. Thus, it is concluded that $\beta$ TiNbSn alloys whose alloy composition is optimized by considering the stability of $\beta$ phase are promising as new biomedical implant materials because of low Young's modulus, and their strength can be increased without degrading low Young's modulus by using the thermo-mechanical processing via stress-induced martensitic transformation.

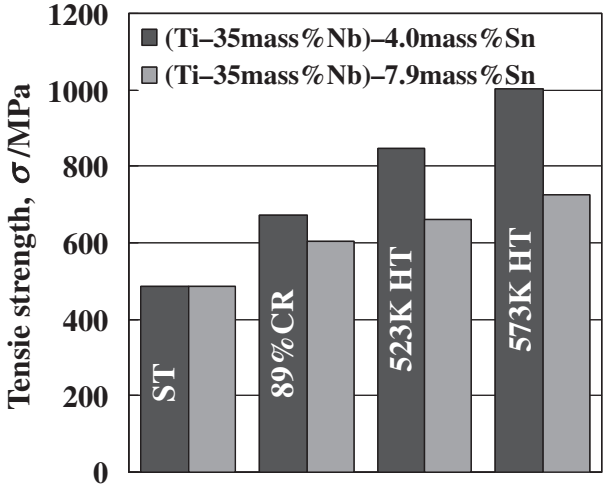


Fig. 13 Tensile strength of (Ti–35 mass%Nb)–4 mass%Sn and (Ti–35 mass%Nb)–7.9 mass%Sn at various conditions.

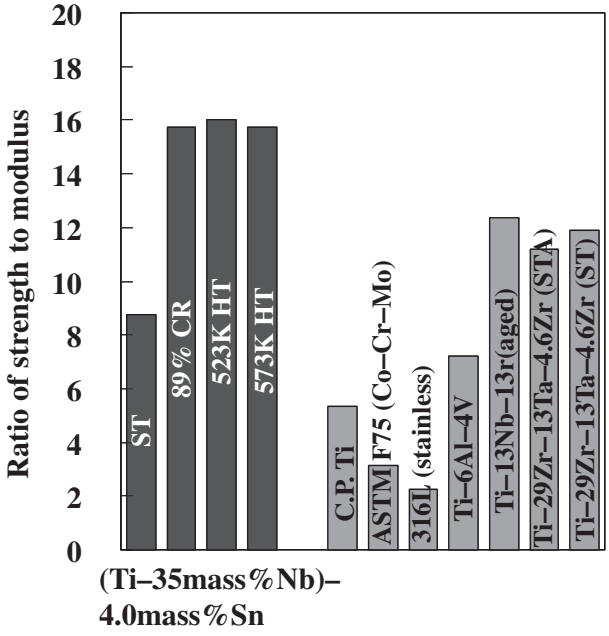


Fig. 14 Ratio of tensile strength to Young's modulus of (Ti–35 mass%Nb)–4 mass%Sn alloy in comparison with some implant materials.

## 4. Summary

Microstructural changes during thermo-mechanical processing and the associated mechanical properties were investigated to develop biomedical $\beta$ Ti alloys with low Young's modulus and high strength using $\beta$ (Ti–35 mass%Nb)–4 mass%Sn and (Ti–35 mass%Nb)–7.9 mass%Sn alloys. The obtained results are summarized as follows.

(1) Stress induced $\alpha''$ martensite phase is formed by cold rolling and reversion to $\beta$ phase is almost completed at 523 K in (Ti–35Nb)–4Sn. Microstructure after reversion consists of fine $\beta$ grains elongated along the rolling direction. Martensite is not stress-induced in (Ti–35Nb)–7.9Sn.

(2) Young's modulus in the rolling direction of solution treated (Ti–35Nb)–4Sn and (Ti–35Nb)–7.9Sn are 55 and 62 GPa, respectively. Young's modulus of 89% cold rolled (Ti–35Nb)–4Sn decreases to 42 GPa, and increases with increasing heat treatment temperature. In contrast, Young's modulus of 89% cold rolled (Ti–35Nb)–7.9Sn exhibits no significant change by cold rolling and subsequent heat treatment.

(3) Young's modulus of solution treated (Ti–35Nb)–4Sn decreases with decreasing temperature toward Ms of 308 K, which is explained by the stability change of $\beta$ phase with temperature. In contrast, Young's modulus of (Ti–35Nb)–4Sn heat treated at 523 K after cold rolling remains almost constant at temperatures between 253 and 423 K, implying $\beta$ stabilization by grain refinement.

(4) $\{211\}_\beta\langle 110\rangle_\beta$ recrystallization texture is evolved in solution treated (Ti–35Nb)–4Sn and (Ti–35Nb)–7.9Sn and $\{110\}_\beta\langle 112\rangle_\beta$ texture is only in (Ti–35Nb)–7.9Sn. After 89% cold rolling, $\{211\}_\beta\langle 110\rangle_\beta$ and $\{100\}_\beta\langle 110\rangle_\beta$ textures are evolved in $\beta$ and $(200)_{\alpha''}[010]_{\alpha''}$ texture is in $\alpha''$ with relation to $\{100\}_\beta\langle 110\rangle_\beta$ texture.

(5) 89% cold rolled (Ti–35Nb)–4Sn exhibits remarkable anisotropy in Young's modulus depending on angle from the rolling direction. This anisotropy is attributable to preferential formation of stress-induced $\alpha''$ martensite variants whose $[010]_{\alpha''}$ with large lattice expansion on $\beta$ to $\alpha''$ transformation is parallel to the rolling direction. Young's modulus does not show significant anisotropy in solution treated (Ti–35Nb)–4Sn and 89% cold rolled and solution treated (Ti–35Nb)–7.9Sn.

(6) Tensile strength of (Ti–35Nb)–4Sn heat treated at 523 K after cold rolling increases over 800 MPa with keeping low Young's modulus of 52 GPa which could be related to work hardening, grain refinement and $\alpha$ precipitation.

## REFERENCES


1) S. Hanada and O. Izumi: Met. Trans. **17A** (1986) 1409–1420.
2) S. Hanada and O. Izumi: Met. Trans. **18A** (1987) 265–271.
3) S. Ishiyama, S. Hanada and O. Izumi: ISIJ International. **32** (1991) 222.
4) S. Ishiyama, S. Hanada and O. Izumi: The Sumitomo Search. **54** (1993) 41–47.
5) T. Ozaki, H. Matsumoto, S. Watanabe and S. Hanada: Mater. Trans. **45** (2004) 2776–2779.
6) D. Kuroda, M. Niinomi, M. Morinaga, Y. Kato and T. Yashiro: Mater. Sci. Eng. A **243** (1998) 244–249.
7) Y. L. Hao, M. Niinomi, D. Kuroda, K. Fukunaga, Y. L. Zhou, R. Yang and A. Suzuki: Metall. Trans. **33A** (2002) 3137–3144.
8) E. Takahashi, T. Sakurai, S. Watanabe, N. Masahashi and S. Hanada: Mater. Trans. **43** (2002) 2978–2983.
9) E. W. Collins: *Physical Metallurgy of Titanium Alloys*, (ASM, Metals Park, OH, 1984).
10) W. F. Ho, C. P. Ju and J. H. C. Lin: Biomaterials. **20** (1999) 2115.
11) C. Baker: Metal Sci. J. **5** (1971) 92–100.
12) T. W. Duerig, J. Albrecht, D. Richter and P. Fisher: Acta Met. **30** (1982) 2161.
13) H. Sasano, T. Suzuki, O. Nakano and H. Kimura: *Titanium'80, Science and Technology*, (AIME, 1980) 717.
14) S. Takai, K. Fukunaga, J. Syarif and T. Tsuchiyama: Mater. Trans. **45** (2004) 2245–2251.
15) Y. L. Zhou, M. Niinomi and T. Akahori: Mater. Sci. Eng. A **371** (2004) 283–290.
16) P. Duwez: Trans. ASM. **45** (1953) 934–940.
17) K. S. Jepson, A. R. G. Brown and J. A. Gray: *The Science Technology and Application of Titanium*, ed. by R. I. Jafee and N. Promisel (Pergamon press, London, 1970), p. 677.
18) H. Kaneko and Y. C. Huang: J. Japan Inst. Metals **27** (1963) 403–406 (in Japanese).
19) A. R. G. Brown, D. Clark, J. Eastabrook and K. S. Jepson: Nature (1964) 914–915.
20) Patent (in Japan), 2004–162171.